A Novel Optical Wireless Modulation exploiting Time, Frequency and Amplitude divisions enabling Link and Illumination Reliability

Andrea Petroni, Antonio Costanzo, Valeria Loscrì, Mauro Biagi

A Novel Optical Wireless Modulation exploiting Time, Frequency and Amplitude divisions enabling Link and Illumination Reliability

Andrea Petroni, Antonio Costanzo, *Member, IEEE*
Valeria Loscri, *Senior Member, IEEE,* and Mauro Biagi, *Senior Member, IEEE*

Abstract

The simultaneous task of data transmission and illumination achievable with Visible Light Communication is continuing to raise the interest of research and industry community. The joint use of the same infrastructure for illumination and communication may enable new location-based services, by implementing sensing functionalities. In this paper, we propose a new multi-dimensional modulation scheme combining different techniques, in order to increase the spectral and energy efficiency, while meeting the optical power emission constraints. Specifically, Pulse Position Modulation Pulse Amplitude Modulation and Frequency Shift Keying are effectively combined in a joint fashion, in order to exploit time, amplitude and frequency information. The innovation of using a smart combination of those modulation formats is based on the exploitation of specific features of the different approaches. In particular, we combine time, amplitude and frequency features to enhance the robustness of the system, without sacrificing the data rate performance as for coded systems. The major implication of such approach is twofold. In this way, we grant a constant illumination level per symbol and, moreover, we outperform in terms of reliability coded modulations for the same level of spectral efficiency. Theoretical results, validated through experimental evaluations, demonstrate that the combined approach achieves very good performance.

Andrea Petroni is with Fondazione Ugo Bordoni (FUB), Viale America, 201 00144 Rome, Italy (e-mail: apetroni@fub.it).

Mauro Biagi is with the Department of Information, Electrical, and Telecommunication (DIET) engineering, "Sapienza" University of Rome, Via Eudossiana, 18 00184 Rome, Italy (e-mail: mauro.biagi@uniroma1.it).

Antonio Costanzo is with LEOST Team at Université Gustave Eiffel, France (e-mail: antonio.costanzo@univ-eiffel.fr).

Valeria Loscri is with FUN Team of Inria Lille, France (e-mail: valeria.loscri@inria.fr).

Index Terms

Modulation, Coding, Illumination, Detection, Optical Wireless

I. Introduction

It is a well recognized matter of fact that the Internet of Everything (IoE) paradigm main limitation is represented by the exiguous wireless resources [1]. In the last decade, Optical Wireless Communication Systems (OWCSs) have risen as a green and effective solution to alleviate the spectral scarcity and boost the ubiquitous deployment and usage of IoE devices [2]. The significant advances in optoelectronic technology have made Light Emitting Diodes (LEDs) and photodetectors (PDs) inexpensive, and efficient hardware to equip optical transceivers [3]. Furthermore, the emission of LEDs can be conveniently managed to provide the illumination service jointly with wireless connectivity. Such scenario is peculiar of the so called Visible Light Communication (VLC) [4], representing one of the most promising fields of application for OWCSs.

By focusing on communication aspects, the design of energy efficient and effective modulation schemes is paramount to maximize the performance in terms of both data rate and reliability [5]. One of the key features of OWCSs is they are Intensity-Modulation/Direct-Detection (IM/DD) systems, requiring high energy efficient modulation techniques. Among the different modulation schemes, one of the most widespread is On-Off Keying (OOK), as a special case of Pulse-Amplitude Modulation (PAM) employing only two transmit signal power levels, one of which is set to zero. In general, even though PAM is very suitable for OWCSs, its main issue is related to the growth of the electrical/optical energy per bit, with the increase of modulation order, necessary to guarantee a certain Bit Error Rate (BER). A higher level of energy efficiency can be achieved with the adoption of orthogonal modulation schemes, although with a negative impact on spectral efficiency. Frequency-Shift Keying (FSK) belongs to the orthogonal modulation schemes category [6]. Its main drawback in the context of OWCSs is represented by its bipolar characteristics, however the variant of FSK based on Direct-Current (DC) offset, namely DC-FSK, allows to obtain a scheme compatible with the IM/DD approach [7]. In fact, from an energy point of view, DC-FSK is more efficient than an asymmetric version of FSK, but suffers from a greater spectral efficiency reduction. Another orthogonal modulation technique is represented by Pulse

Position Modulation (PPM) [8]. PPM is interesting for OWCSs since particularly fitting also for localization purposes, but its inefficiency concerns the peak-to-mean optical power ratio [9].

Based on these premises, it is clear that each modulation scheme has its own strengths and weaknesses. Hence, combining different techniques would be a promising approach to capitalize on the benefits and mitigate drawbacks. One of the earliest proposal for hybrid schemes is described in [10], where a low-density parity-check coded hybrid subcarrier-amplitude-phase-polarization modulation is investigated to deal with optical channels and providing up to 240-Gb/s rate. Another work about hybrid solutions for OWCSs has been presented in [11]. The authors propose a class of optical modulation techniques as a combination of PPM and FSK and with the addition of a polarization component and/or phase modulation, demonstrating the achievement of a higher power efficiency. Both the schemes in [10], [11] were developed for optical systems, but not specifically wireless, hence potential issues related to dimming control, typical of indoor VLC, are not addressed. A hybrid DC Frequency and Phase Shift Keying modulation scheme for optical wireless systems has been investigated in [12]. The authors established the particular combination of phase and frequency leading to an optimal energy and spectral efficiency. Phase and frequency shift applied to OOK are considered by the authors in [13] to demonstrate the feasibility of a 160 meters outdoor VLC link, by employing an image sensor-based receiver for reliable signal detection. Still dealing with free space optics (FSO), the joint use of quadrature amplitude modulation and multi-pulse position modulation is evaluated in [14] for both turbulence-free and gamma–gamma channels, with results demonstrating its superiority to other known schemes in terms of power efficiency and outage probability. Although the techniques in [12]–[14] are tailored to optical wireless communications, no focus has been made on their application in indoor VLC systems, therefore performance related to lighting control were not investigated. An interesting contribution on hybrid modulation schemes has been proposed in [15], where the authors combine Pulse Width Modulation, PPM and Discrete Pulse Amplitude Modulation (DPAM) in order to increase the data transmission rate. Furthermore, the use of DPAM is also aimed to achieve the dimming function. Similarly, the features of DPAM and the reliability of variable PPM are jointly exploited in [16] to improve the communication rate while providing illumination control as well. The effectiveness of the approaches presented in [15] and [16] was validated through several experiments, however the lack of preliminary simulation analysis does not allow the measured performance to be compared with a reliable benchmark. Besides in [17] a new modulation format able to constrain macro-symbol by macro-

symbol the lighting level has been proposed by merging PAM and PPM. The receiver is really complex and a sub-optimal solution has been proposed in [18].

Based on the encouraging results available in the literature, the idea of this work is to explore the potentialities of three popular modulation formats and try to merge them in a whole framework. Hence, in this work we propose a joint multi-modulation scheme, based on the combination of non-orthogonal PPM, PAM and FSK, in order to efficiently exploit the time, amplitude and frequency features of the different schemes.

More in detail, it is known from theory [19] that the adoption of spectrally efficient *pure* modulations like PAM allows the achievement of high data rates. However, the main drawback concerns the power inefficiency that, in OWCSs, does not guarantee the provision of a constant lighting level per symbol and, moreover, modulation only is not sufficient to achieve high reliability in real systems. Nonetheless, solving the reliability problem through coding does not allow to solve illumination issues. On the other hand, light emission and robustness to errors can be effectively addressed by using different schemes, such has FSK or PPM, but rate is unavoidably penalized due to the bandwidth inefficiency.

With the aim to achieve a convenient compromise between rate and reliability, the use of hybrid modulations has been recently spreading. Current works in the literature mainly deal with the merging of pairs of modulation schemes, typically phase and amplitude, frequency and amplitude, phase and frequency domains. Furthermore, the largest part of the proposed solutions are developed for FSO applications or, in general, not specifically for indoor wireless scenarios. Hence, issues related to power and illumination control that characterize indoor VLC are still very often neglected.

The main novelty of this work is that we propose a multi-modulation scheme relying on the combination of non-orthogonal PPM, PAM and FSK to leverage the specific features and smartly mitigate the main drawbacks of each modulation. Such popular schemes are merged in a whole, novel framework, in order to efficiently exploit the time, amplitude and frequency features of the different schemes. The goal is to achieve performance improvements in terms of spectral and power efficiency with respect to pure modulations, providing also a constant illumination level that represents a fundamental requirement in real-world indoor VLC systems.The main contributions can be summarized as follows. The multi-dimensional modulation we propose:

- is able to simultaneously *exploit* the spectral efficiency of PAM and the power efficiency of PPM and FSK by combining them in a single and more effective scheme, where the impact

of pure modulations weaknesses is reduced;

- is able to grant a constant power level, thus meaning constant lighting level on a per symbol basis, allowing illumination control while other coded and uncoded schemes generally do not;
- allows the use of different receivers, ranging from the optimum to several sub-optimal ones, with each one providing a particular trade off between computational complexity and performance;
- is able to outperform block coding strategies, for the same level of spectral efficiency, in terms of communication reliability, as confirmed by experimental validation as well.

The paper is organized as follows. In Sec.II, we introduce the system model, including channel description and the multi-dimensional modulation we propose. In Sec III, we detail the optimum receiver structure and discuss the implementation of several sub-optimal and less costly receivers. In order to evaluate both the performance of the modulation itself and the different receivers effectiveness, we proceed in Sec. IV with the numerical results description and we also show some test results. Last, in Sec. V we draw final conclusion.

II. System model and proposed modulation

Let us consider a point-to-point optical link with transmitter and receiver equipped with a single LED and PD, respectively. The signal propagation can be modeled as:

$$y(t) = \rho h x(t) + w(t) \tag{1}$$

where $x(t)$ is the instantaneous power associated to the transmitted optical signal, h accounts for the channel effect from the source to the receiver, ρ is the responsivity of the PD (measured in ampere/watt), and $y(t)$ is the received current signal resulting from opto-electrical conversion. Finally, $w(t)$ is the noise term modeled as zero-mean, additive white and Gaussian, the variance of which is indicated as σ_w^2. Regarding the channel characterization, by assuming the signal propagation as Lambertian and line-of-sight, we can model h as [20]:

$$h = \begin{cases} \dfrac{(n+1)A_{\text{pd}}}{2\pi D^2}\cos^n(\phi)\cos(\psi)g(\psi), & \psi \leq \Psi \\ 0, & \psi > \Psi \end{cases} \tag{2}$$

where A_{pd} is area of the PD, D is the distance between LED and PD, g represents the gain of a potentially employable optical concentrator and $n = -\ln 2/\ln(\cos\Phi_{1/2})$ represents the

Lambertian emission factor derived from the LED -3dB semi-angle. Finally, ϕ and ψ are the angle of radiance and incidence, respectively, with Ψ defining the PD FOV.

Herein, we propose a novel multi-dimensional modulation scheme based on a PPM-like signaling, FSK-inspired shape and also PAM-based modulation. The general framework description is provided in Figure 1. Transmit side operations are described in the current section, while received signal processing is detailed in the next one.

Now, we proceed by first introducing the generic symbol emitted by the modulator in the following compact form:

$$x(t) = I_0 + A_m s_n(t - \ell T_c) \tag{3}$$

where I_0 is a light bias that is used to maintain constant the lighting level per symbol. This choice is fundamental in order to guarantee a constant illumination level. In fact, the use of

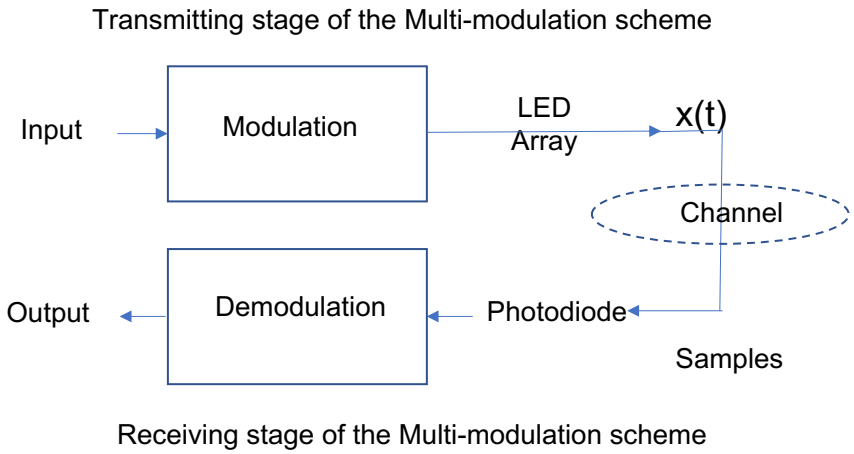

Fig. 1. General framework describing the proposed scheme principles.

different amplitudes, as realized in PAM modulation, allows to have a constant *average* lighting, only under the hypothesis of equal distribution of the transmitted symbols. Unfortunately, such assumption *fails to be verified*, for example when an image characterized by black and white stripes has to be transmitted. There, we have several consecutive and identical symbols to be transmitted, so reflecting in LEDs on the same power level for several time instants, including the level zero corresponding to the source switch off. It is worth specifying that I_0 and $s_n(t)$ represent current signals that, by assuming ideal electro-optical conversion at transmit side, define the optical signal $x(t)$. Still regarding eq. (3), A_m is one of the M amplitudes belonging

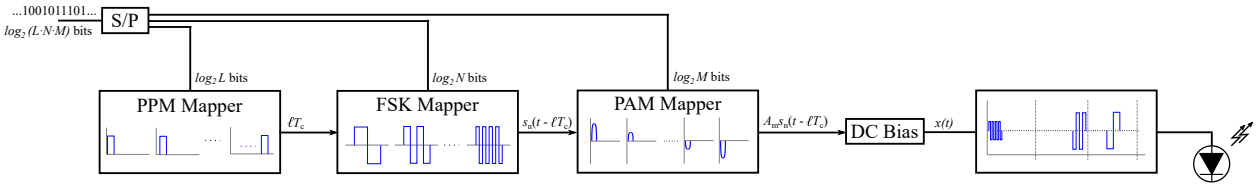

Fig. 2. Block diagram of the PPM-FSK-PAM modulator.

to the PAM-based alphabet $\mathcal{A} = \{A_0, A_1, ..., A_{M\text{-}1}\}$, T_c is the elementary PPM-like delay and the index $\ell = 0, 1, ..., L\text{-}1$ rules the signal time shift according to one of the L possible PPM delays gathered in $\mathcal{L} = \{0, T_c, ..., (L-1)T_c\}$. Finally, $s_n(t)$ is the square wave describing the N-FSK signal shape, with n=1,2,...,N indicating the number of wave cycles within the signaling time T_p. In detail, $s_n(t)$ can be represented as:

$$s_n(t) = \sum_{k=1}^{n} \left(rect\left(\frac{t - T_p/4n - (k-1)T_p/2n}{T_p/2n} \right) - rect\left(\frac{t - T_p/4n - kT_p/2n}{T_p/2n} \right) \right) \tag{4}$$

where the first term is the positive portion of the square wave and the second term represents the negative component of the square wave. The modulator combining the principles of PPM, FSK and PAM signaling is depicted in Fig. 2, while a graphical example of symbol emission is reported in Fig.3. Once more, it is possible to appreciate that the symbol power is constant, hence, the illumination has a constant value on a symbol basis. Given T_c and T_p, the use of L possible delays, N possible frequencies and M possible amplitudes entails the overall symbol time to be equal to $T_s = T_p + (L-1)T_c$ (it is worth clarifying that the PAM modulation does not impact on the symbol duration, but only on amplitude). Interestingly, it can be noted that if $T_c = T_p$ the orthogonal PPM signaling is realized, while $T_c < T_p$ returns non-orthogonal PPM. In this direction, by expressing $T_c = \beta T_p$, with $0 < \beta \leq 1$ ($\beta = 1$ representing orthogonal PPM), the spectral efficiency of the proposed modulation format (related to the electrical signal) is given by:

$$\eta = \frac{\log_2(L \cdot N \cdot M)}{N(1 + \beta(L-1))}. \tag{5}$$

According to the modulator block diagram in Fig. 2, the bit mapping can be done by composing the bit string related to the generic symbol as $\log_2(L \cdot M \cdot N)$ bits where the first $\log_2 L$ are related to PPM, the second $\log_2 N$ are linked to FSK and the last $\log_2 M$ deal with PAM.

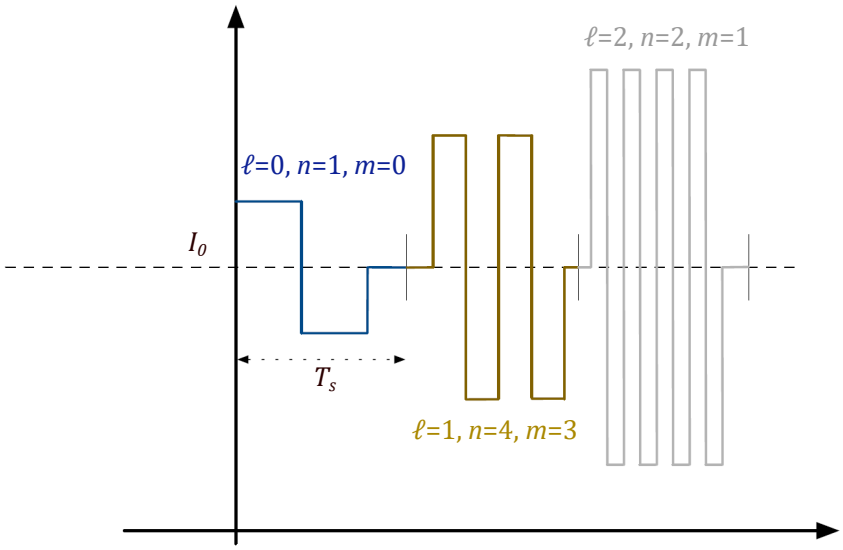

Fig. 3. Graphical representation of modulated symbols with different combinations of ℓ, n and m.

It is worth highlighting that the proposed scheme combines a highly spectrally efficient modulation such as PAM with spectrally inefficient but reliable modulation like PPM and FSK. In this regard, PPM and FSK realize a sort of coding (even though here no channel coding is present) as they provide a higher robustness to errors with respect to pure PAM signaling, that is unavoidably paid in terms of spectral efficiency reduction. In fact, by looking at eq. (5), the use of PAM signaling ($M > 1$) allows η to increase, while the presence of PPM and FSK ($L > 1$, $N > 1$) lowers η. Moreover, β ruling the width of PPM delay impacts on the trade off between spectral efficiency and reliability as well. Another interesting aspect to highlight is that, by smartly combining the three different techniques, we are able to improve energy efficiency. In particular, energy efficiency is meant as the system is able to reduce the BER in correspondence to the same SNR values, thus requiring lower power to achieve the same performance of other schemes.

III. Digital demodulation: optimal and sub-optimal receivers

As detailed in the previous section, by combining PPM, FSK and PAM we realize a multi-dimensional modulation scheme jointly exploiting time, frequency and amplitude domains. Regarding digital demodulation, we must anticipate that the relationship that links PPM, FSK and PAM still holds. In fact, a possible wrong decision about the PPM part of the symbol may induce

errors both in symbol frequency and amplitude detection. An unreliable decision on the FSK part may lead PAM detection to be unreliable as well. Finally, having many close signal amplitudes available makes PAM detection very challenging, and errors may have also a significant impact on PPM symbol part recognition.

Such a *circular* dependency among PPM, FSK and PAM suggests that *parallel detection* of the three modulation components can not be followed. Therefore, a different approach combining time, frequency and amplitude dimensions is required. In this regard, we resort to the principles of Maximum Likelihood (ML) criterion allowing symbol detection to be described as follows. First, the transmit signal model in eq. (3) allows eq. (1) to be rewritten as:

$$y(t) = \rho h I_0 + \rho h A_m s_n(t - \ell T_c) + w(t) \tag{6}$$

from which it is possible to recover the unbiased continuous time received signal as:

$$y_u(t) = y(t) - \rho \tilde{h} I_o = \rho h A_m s_n(t - \ell T_c) + w(t) \tag{7}$$

where the term $\tilde{h}$ is the estimated version of the channel that, under the hypothesis of reliable estimation, leads to have the $y_u(t)$ with zero-mean. As previously outlined, the bits carried by PPM, FSK and PAM must be decoded in a joint fashion. The most effective, but also expensive, way to achieve this goal is to implement the so called optimum receiver (OR) [19], based on signal filtering operated by considering all the possible combinations of PPM, FSK and PAM signals. As alternatives, we present three sub-optimal receivers, referred as quasi-optimum receiver (QOR), direct receiver (DR) and feedback receiver (FBR), respectively. Below, we detail the characteristics of the mentioned receivers, discussing the different trade off between complexity and performance provided by each configuration.

A. Optimum receiver

By looking at the scheme of the OR reported in Fig. 4 (excluding the gray section), it is possible to appreciate that, by employing L-PPM and N-FSK, $L \cdot N$ filters matched to different delays and frequencies are required in order to evaluate the corresponding $L \cdot N$ decision metrics, given as:

$$r_{\ell,n} = \frac{1}{T_p} \int_{\ell T_c}^{\ell T_c + T_p} y_u(t) s_n(t - \ell T_c) dt \tag{8}$$

with n=1,...,N, ℓ=0,...,L-1. Then, the decision related to the PPM-FSK symbol components is taken according to the following rule, that allows to obtain the pair $(\hat{\ell}, \hat{n})$:

$$\hat{\ell}, \hat{n} = \underset{\ell=0,...,L\text{-}1,\ n=1,...,N}{\operatorname{argmax}} |r_{\ell,n}|. \tag{9}$$

representing the indexes of the decided PPM and FSK symbols, respectively. It is important to highlight that, in eq. (9), we introduce the use of modulus on $r_{\ell,n}$ since the electrical signal, for what concerns the amplitude, can be negative due to the presence of noise. Differently, measuring only the maximum on $r_{\ell,n}$ may lead to totally misdetect the frequency component.

At this stage, once decided $\hat{\ell}$ and $\hat{n}$, only the PAM component still needs to be detected. Hence, by resorting to the ML criterion based on Euclidean distance, we can perform the PAM detection according to the following rule:

$$\hat{m} = \underset{m=0,...,M\text{-}1}{\operatorname{argmin}} (\rho\tilde{h}A_m - r_{\hat{\ell},\hat{n}})^2 \tag{10}$$

so that $\hat{\ell}$, $\hat{n}$ and $\hat{m}$ return the decided indexes of the PPM, FSK and PAM symbols composing the transmitted multi-dimensional symbol.

Summarizing, we can define the computational cost required by the OR as $\mathcal{O}_{\text{OR}} = L \cdot N + M$, given by the $L \cdot N$ filtering operations related to PPM and FSK detection plus the M metrics computations for PAM detection. As the decision on the received multi-dimensional symbol is taken by comparing it to all the possible symbols belonging to the PPM-FSK-PAM alphabet, the OR results as the best performing receiver. On the other hand, the required computational cost $\mathcal{O}_{\text{OR}}$ may be high, especially if the modulation orders grow.

B. Quasi-optimum receiver

The block diagram of the sub-optimal QOR is the same of the OR, but including a further processing part, highlighted in the gray area in Fig. 4, realizing a very first decision stage that allows the overall signal processing to be reduced with respect to the case related to the OR. In fact, the receiver is referred as *quasi-optimum* since, whenever possible, it avoids the full computation of the filtering operations characterizing the OR. In QOR, the initial processing stage is characterized by an energy detector that computes the signal energy over the L PPM time windows characterizing the received signal $y_u(t)$. So, we have that the quantity:

$$\xi(\ell) = \int_{\ell T_c}^{\ell T_c + T_p} |y_u(t)|^2 dt,\ \ \ell = 0, ..., L\text{-}1 \tag{11}$$

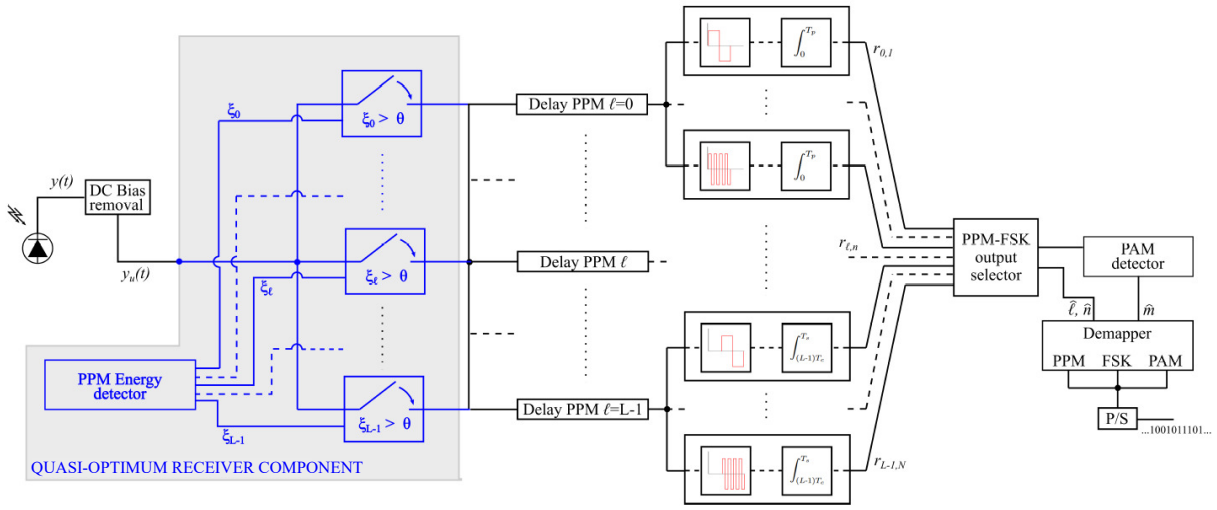

Fig. 4. Block diagram of optimum receiver (OR) and quasi-optimum receiver (blue QOR).

represents the signal energy referred to the ℓ-th PPM slot measured in $y_u(t)$. Once the L energy metrics are calculated, a threshold θ is used to determine the best candidates to be the detectable PPM symbols, gathered in the set $\mathcal{L}_\theta = \{\ell \mid \xi(\ell) > \theta\}$. Hence, the PPM-FSK symbol is detected according to the following rule:

$$\hat{\ell}, \hat{n} = \underset{\ell \in \mathcal{L}_\theta,\ n=1,\ldots,N}{\operatorname{argmax}} |r_{\ell,n}| \tag{12}$$

where the maximum is not searched in the set characterized by $L \cdot N$ elements (as done in the optimum receiver case), but in a number of $|\mathcal{L}_\theta| \cdot N$. Please notice that, in this case, the operator $|.|$ applied to the set $|\mathcal{L}_\theta|$ means its cardinality, that is, the number of elements that it is composed of. As in general $\mathcal{L}_\theta \leq L$, the number of metrics computed according to eq. (8) is lower in QOR than in the optimal receiver, thus saving computational effort.

The setup of the threshold θ depends on the energy level expected to be measured within the PPM slot where the FSK signal is placed on. In this regard, let us assume the transmission of a pilot multi-dimensional symbol $x_{\mathrm{P}}(t)$ where ℓ, n and m are known. The estimated energy, calculated as in eq. (11) in the ℓ-th PPM slot and referred as ξ_{P}, can be exploited to define the threshold theta as $\theta = (1-\beta)\xi_{\mathrm{P}}$, that essentially represents the energy level expected in the $(\ell+1)$-th PPM slot immediately next to that one where the signal is placed on. In fact, due to

their closeness, the ℓ-th PPM symbol is likely to be confused with the $(\ell+1)$-th one, so this is why the threshold θ is set as a function of the energy expected on the $(\ell+1)$-th PPM slot.

Finally, concerning the detection of the PAM symbol, we proceed in the same way reported in eq. (10). Overall, the processing cost related to the QOR is $\mathcal{O}_{\text{QOR}} = L + \mathcal{L}_\theta \cdot N + M$, given by the L filtering operations characterizing the PPM energy detector, $\mathcal{L}_\theta \cdot N$ filters for PPM and FSK detection, and finally M metrics computations related to PAM decision. It is worth noting that $\mathcal{O}_{\text{QOR}}$ is not a fixed value since it strongly depends on the number of elements composing the set $\mathcal{L}_\theta$.

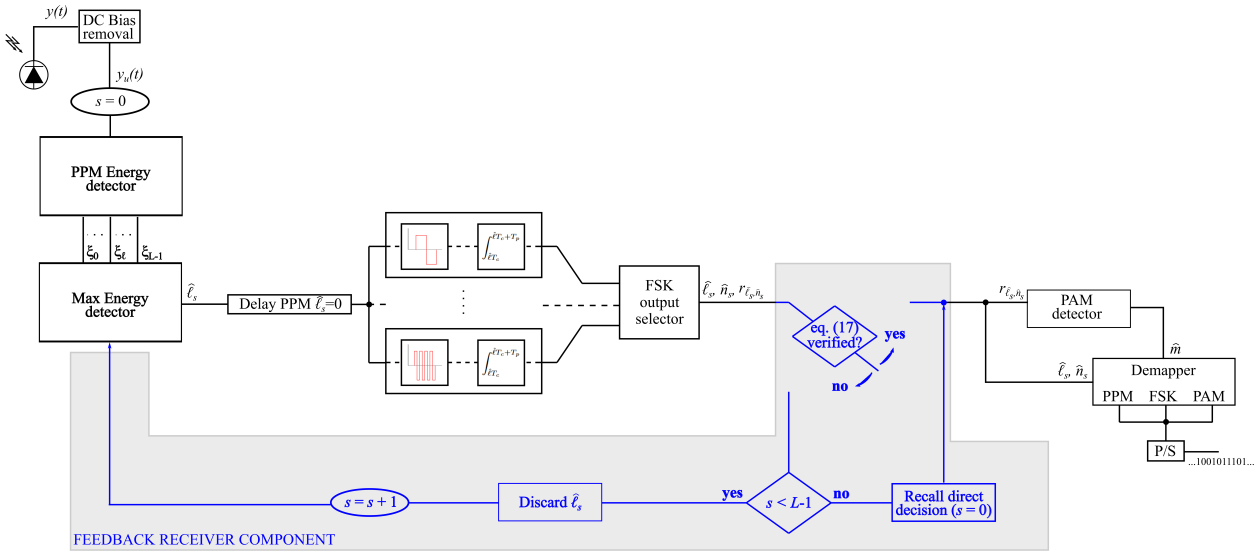

Fig. 5. Block diagram of direct receiver (DR) and feedback receiver (FBR).

C. Direct receiver

The receiver introduced as DR is probably the less complex sub-optimal solution in terms of computational cost since signal detection is performed sequentially, starting from the PPM-related part, then moving to FSK and finally to PAM parts. The use of such detection approach is the reason why the receiver is referred as *direct*. For the sake of clarity, we would remark that, in this case, detection is not operated jointly on the PPM, FSK and PAM signal components. The block diagram of DR is depicted in Fig. 5 (excluding the gray box). Regarding PPM detection, an energy detector as that one introduced in eq. (11) is considered, so as:

$$\hat{\ell} = \max_{\ell=0,\dots,L\text{-}1} \xi(\ell) \tag{13}$$

returns the index of the decided symbol related to the PPM part. From $\hat{\ell}$ it is possible to identify the time delay characterizing the FSK signal $s_n(t)$ within the received symbol $y_u(t)$, so that the FSK detection can be performed according to the following rule:

$$\hat{n} = \underset{n=1,\ldots,N}{\operatorname{argmax}} |r_{\hat{\ell},n}| \tag{14}$$

where it is important to highlight that we are not dealing with $r_{\ell,n}$ as in eq. (8), but with $r_{\hat{\ell},n}$ defined as:

$$r_{\hat{\ell},n} = \frac{1}{T_p} \int_{\hat{\ell}T_c}^{\hat{\ell}T_c+T_p} y_u(t) s_n(t - \hat{\ell}T_c) dt. \tag{15}$$

In other words, eq. (15) defines the filtering operations that consider only the specific time delay given by $\hat{\ell}$, while filtering in eq. (8) is performed for ℓ=0,1,...,L-1. Finally, for what concerns PAM detection, we can still resort to the ML based approach followed in eq. (10).

Regarding the DR, the number of filtering operations and comparisons requested for symbol demodulation is really low since, as previously outlined, detection is performed sequentially on the PPM, FSK and PAM parts. Therefore, the required computational cost is given as $\mathcal{O}_{\text{DR}} = L + N + M$.

D. Feedback receiver

The last receiver we propose is referred as FBR and it is somewhat similar to the DR. In fact, its reference block diagram is that one reported in Fig. 5, but including the gray area as well. With FBR, it is possible to take a temporary decision on the PPM-FSK symbol part, with the detection being potentially performed multiple times iteratively. Therefore, as highlighted in Fig. 5, a feedback-like mechanism is realized and integrated in the DR architecture. In this regard, we indicate the iteration number with the subscript s, so that $\hat{\ell}_s$ refers to the PPM symbol part decided at the s-th detection iteration. For s=0, we have the very first decision on PPM as taken according to eq. (13) similarly to the DR case. Even for FSK detection, for s=0, $\hat{n}_s$ is determined as in eq. (14) representing the maximum output of matched filtering. Differently from DR, we also consider a second potential candidate to be the decided FSK symbol, formally defined as:

$$\hat{n}_s^{\diamond} = \underset{n \in \mathcal{N}/\{\hat{n}_s\}}{\operatorname{argmax}} |r_{\hat{\ell},n}| \tag{16}$$

that is the second-highest output of eq. (15) (in other words, maximum output of matched filtering excluding $\hat{n}_s$). Given such two candidates, $\hat{n}_s$ is recognized as a reliable decision if the following conditions are simultaneously met:

$$|r_{\hat{\ell}_s,\hat{n}_s}| - |r_{\hat{\ell}_s,\hat{n}_s^\diamond}| > \Psi \tag{17a}$$

$$|r_{\hat{\ell}_s,\hat{n}_s}| > \Gamma. \tag{17b}$$

Specifically, eq. (17a) is used to explicitly verify the accuracy of FSK decision. In fact, if the difference between $\hat{n}_s$ and $\hat{n}_s^\diamond$ is larger than a suitably defined threshold Ψ, it follows that the computing of N matched filters returns an output, namely $\hat{n}_s$, significantly higher than the others. So, it is likely that $\hat{n}_s$ correctly identifies the index of the received FSK symbol. The reference threshold is defined as $\Psi = 0.25(A_{\text{M-1}} - A_0)/(M-1)$ and is function of the distance expected between adjacent PAM amplitudes, with 0.25 being an empirically chosen scaling factor. Eq. (17b) allows not only to explicitly verify the reliability of FSK detection, but also to understand if the decision on PPM has been taken correctly. In this regard, if the N matched filters computed for FSK detection returns very low output values, it may be that a wrong decision on PPM has led to a misaligned identification of the FSK signal within $y_u(t)$, causing the FSK filtering to be *unmatched*. On the other hand, if the highest filter output $r_{\hat{\ell}_s,\hat{n}_s}$ exceeds a certain threshold Γ, conveniently chosen to deal with energy detector behavior, it is likely that the PPM detection has been performed reliably. To this aim, the threshold has been set as $\Gamma = 0.25|A_{\text{min}}|$, with A_{min} being the minimum amplitude for a PAM symbol and 0.25 representing a scaling factor as for Ψ. Therefore, the joint meeting of eqs. (17a)-(17b) should prevent from a wrong decision on the PPM-FSK symbol pair ($\hat{\ell}_s$,$\hat{n}_s$).

Otherwise, if eq. (17) is not met, we consider the next step for s, that is the next iteration, and we get back to the energy detection stage by evaluating:

$$\hat{\ell}_{s+1} = \max_{\ell \in \mathcal{L}/\{\hat{\ell}_0,\ldots,\hat{\ell}_s\}} \xi(\ell) \tag{18}$$

that is a new decision on the PPM symbol part, but excluding the index $\hat{\ell}_s$ found during the previous iteration. Once the *new* decided PPM symbol is available, we proceed again with FSK detection by computing eqs. (13)-(16) and checking if, given $\hat{\ell}_{s+1}$, eq. (17) is finally met. Such procedure is repeated until eq. (17) is verified or, at most, L times corresponding to the maximum number of decisions that can be considered for PPM, thus realizing the feedback path highlighted in Fig. 5. Just in case eq. (17) is never achieved, the final symbol decision will be the one related

to the iteration $s = 0$. Finally, dealing with PAM detection, still we can resort to eq. (10).

It is important to note that in FBR, as for QOR, the number of filtering operations and symbol comparisons is not fixed since it depends on the meeting of conditions in eq. (17). Hence, the cost is $\mathcal{O}_{\text{FBR}} = L + (s+1) \cdot N + M$ where the fixed terms L and M are related to the implementation of the PPM energy detector and PAM detector, respectively, while the remaining variable term is function of the number of feedback iterations.

Remark - about the possible receiver selection

Although the implementation of DR is worth for what concerns cost, the optimal receiver allows to achieve the minimum error rate, thus granting the highest level of reliability. Hence, the use of the most convenient receiver can be seen in two different ways. First, if the setup is fixed and it is expected that no significant changes are applied to the communication link, once assigned the parameters, it is possible to select the receiver allowing the achievement of the requested target performance in terms of error rate, while optimizing the receiver computational effort. This represents an offline solution. Second, if the channel is subject to variations (for example a user moving in a room), the received optical power changes and so the signal-to-noise ratio (SNR). This implies that, if the receiver is implemented by software, it is possible to realize a SNR threshold based detection method tuning, so that the channel conditions drive the most convenient receiver selection. By doing so, the requested reliability level can be provided at the lowest processing cost. We comment further in the numerical results section the possible use of the receiver selection procedure.

IV. Numerical results

In this section, we investigate the performance of the proposed multi-dimensional modulation scheme, highlighting the benefits brought by the use of such approach in terms of both communication reliability and illumination control. Furthermore, we evaluate the effectiveness of the three sub-optimal receivers presented in the previous section, discussing the trade off between computational complexity and error rate achievable with respect to the optimum receiver case. Matlab software was employed for simulating the transmission of 10^7 symbols over a point-to-point optical link. In addition, some results obtained from experimental validation are also reported and discussed. Different communication distances between transmitter and receiver have

been considered so as to investigate the performance as a function of the average electrical SNR per symbol, formally defined as:

$$\gamma = \frac{1}{K_s} \sum_{i=0}^{K_s\text{-}1} \frac{(\rho P_i h)^2}{\sigma_w^2} \tag{19}$$

where $K_s = L \cdot N \cdot M$ is the size of the considered multi-dimensional modulation vocabulary and P_i is the power of the i-th transmitted symbol, with $i = 0, 1, 2, ..., K_s$-1. For simulations, we considered normalized LED and PD parameters since performance are evaluated as a function of SNR. On the other hand, a detailed description of hardware parameters and setup is provided when presenting the experimental results.

A. Optimum and Multi-dimensional modulation performance

As outlined in Sec. II, the multi-dimensional modulation allows the high spectral efficiency of PAM to be combined with the reliability of PPM and FSK, to achieve good data rates while providing robustness to errors. In this direction, we now compare the BER performance of uncoded and coded PAM with some PPM-FSK-PAM schemes.

Comparison with uncoded strategy: We selected some modulation formats providing a target spectral efficiency η^*=1 bit/s/Hz and η^*=2 bit/s/Hz achieved with 2-PAM (or OOK) and 4-PAM, respectively. Such PAM formats have been taken as a reference since being the most widespread in OWCS [21], [22]. In fact, the optical signal starts suffering from high attenuation after few decades of centimeters propagation, therefore using higher order PAM modulations results as unreliable due to the detection errors caused by the presence of noise.

Given η^*=1 bit/s/Hz, 2-PAM has been compared to 2-PPM/2-FSK/2-PAM with β=0.5, to 4-PPM/2-FSK/4-PAM with β=0.5 and to 16-PPM/4-FSK/2-PAM with β=0.05. The BER results are plotted in Fig. 6(a), with curves related to the multi-dimensional modulations being obtained considering the OR based detection. In particular, it can be appreciated that the multi-dimensional modulations characterized by 16-PPM/4-FSK/2-PAM and 2-PPM/2-FSK/2-PAM are able to outperform 2-PAM, while 4-PPM/2-FSK/4-PAM provide worse performance. Such results can be explained as follows. By recalling eq. (5), the use of PPM and FSK (that is, $L > 1$ and $N > 1$) lowers the spectral efficiency. So, there is a limited number of combinations of L, N and β that guarantee the achievement of the target η^*. Moreover, the spectral efficiency reduction caused by the use of PPM and FSK must be counterbalanced by increasing the PAM modulation order as well. This is what happens when dealing with the considered 4-PPM/2-FSK/4-PAM case.

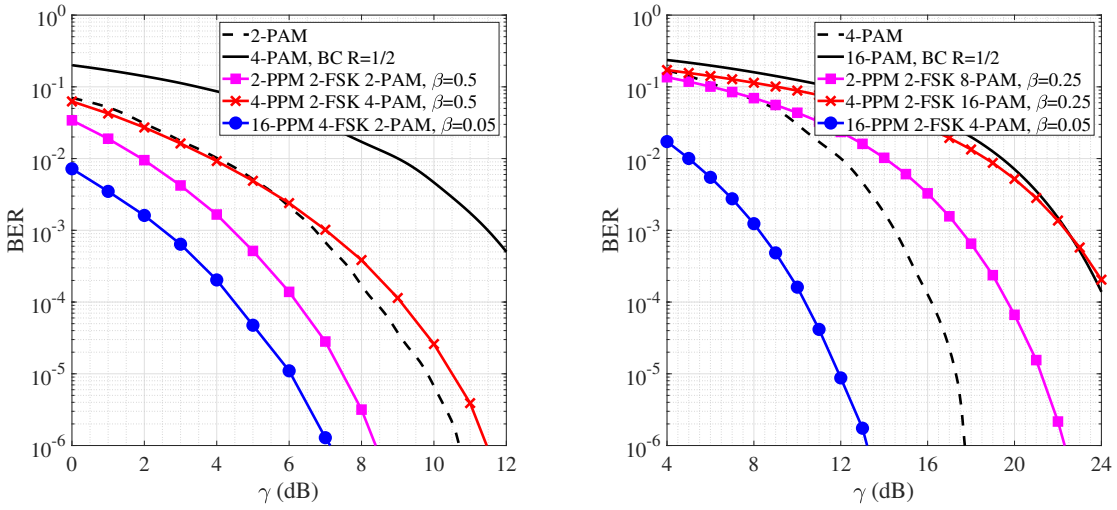

(a) Target $\eta^* = 1$ bit/s/Hz

(b) Target $\eta^* = 2$ bit/s/Hz

Fig. 6. BER performance, based on the OR, of different modulation schemes providing the same spectral efficiency η^*.

Unfortunately, the use of PPM and FSK to achieve a higher reliability requests the PAM order M to be increased up to 4 so as to guarantee η^*=1 bit/s/Hz. Hence, the benefits brought by PPM and FSK in terms of robustness to errors are *lost* since the use of 4-PAM leads the communication to be more sensitive to errors than an uncoded 2-PAM. As a consequence, such kind of multi-dimensional modulation is not convenient with respect to 2-PAM.

Moving to a more challenging case, Fig. 6(b) shows the BER for those schemes providing a target spectral efficiency η^*=2 bit/s/Hz, that are uncoded 4-PAM, 2-PPM/2-FSK/8-PAM with β=0.25, 4-PPM/2-FSK/16-PAM with β=0.25 and to 16-PPM/2-FSK/4-PAM with β=0.05. Curves still refer to the performance achieved with the OR. Even in this case, it can be observed that 2-PPM/2-FSK/8-PAM and 4-PPM/2-FSK/16-PAM are not feasible since the introduction of PPM and FSK requires the increase of the PAM order to achieve the desired spectral efficiency. So, as discussed before, the benefits of PPM and FSK are *canceled* by the use of an unreliable PAM order.

Comparison with coded strategy: An easy comment and objection is that, in order to grant reliability, a coding strategy may be applied, obviously at the cost of spectral efficiency reduction since a part of the bits sent on the channel are for error correction. In this regard, we proceed with an additional performance comparison that is related to block coding (BC) with coding rate R=1/2, thus meaning that the ratio between the number of bits entering in the coder are half of

the ones out the coder. In order to provide a comparison for the same spectral efficiency η^*=1 bit/s/Hz, we considered 4-PAM. As just mentioned, the role of channel coding is to improve the robustness to errors, but at the expense of rate reduction. Therefore, the achievement of the target spectral efficiency requests the PAM order to be necessarily increased. From the results, we can appreciate that the performance of coded 4-PAM are significantly lower than uncoded 2-PAM, thus revealing that the proposed multi-dimensional modulation is more convenient than coding. Of course, many other coding schemes may be considered, but the achievement of good performance unavoidably requires the decoding strategy complexity increase. Differently, in 16-PPM/4-FSK/2-PAM with β=0.05 and 2-PPM/2-FSK/2-PAM with β=0.5 the PAM order remains the lowest possible, while PPM and FSK are introduced to achieve a higher reliability. In fact, these solutions result as better performing than uncoded 2-PAM even though providing the same spectral efficiency. In Fig. 6(b), the same problem concerns 16-PAM with block coding and R=1/2, where the unreliability of the high PAM modulation order can not be properly counterbalanced by coding. On the other hand, the implementation of a 16-PPM/2-FSK/4-PAM results to be more convenient than an uncoded 4-PAM, thus meaning that PPM and FSK are exploited fruitfully to achieve a lower BER.

Results Discussion

Interestingly, it can be noted from Fig. 6 that the most reliable modulation schemes to achieve both η^*=1 bit/s/Hz and η^*=2 bit/s/Hz consider the use of a high PPM order equal to L=16, that may induce a significant spectral efficiency decrease according to eq. (5). However, in both cases we have β=0.05 allowing the realization of a non-orthogonal PPM, which provides a lower spectral efficiency reduction with respect to orthogonal PPM (where β=1). Furthermore, it is worth highlighting that, in general, when dealing with the proposed multi-dimensional modulation, using high PPM modulation formats may be more convenient than increasing the FSK order. In fact, regarding PPM, we have two degree of freedom to adjust the spectral efficiency, that are L and β. On the other hand, FSK performance are ruled by the unique parameter N. Hence, by increasing N the spectral efficiency decreases, but there is no other way to mitigate such reduction, as happens in PPM by adjusting β.

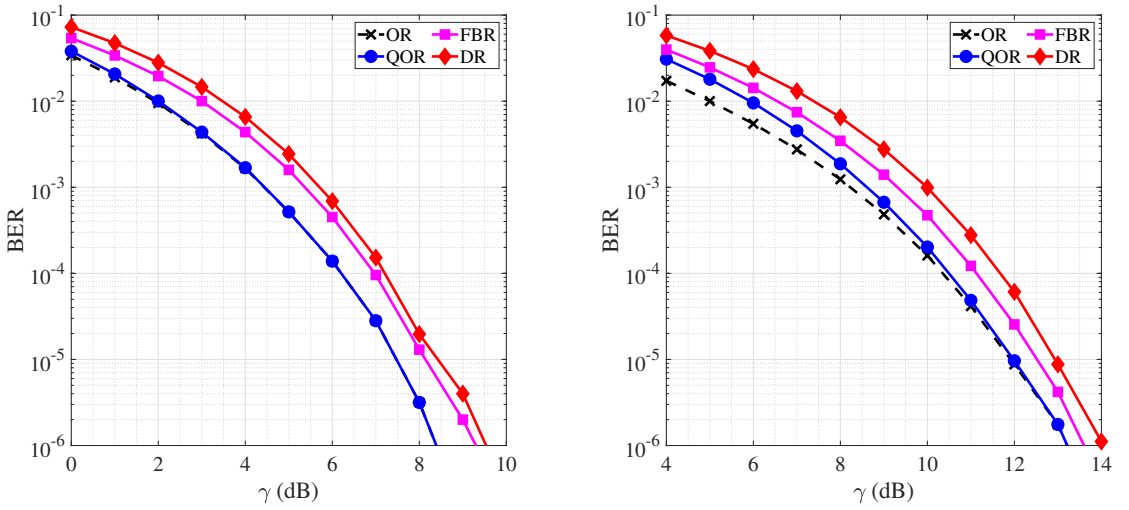

(a) 2-PPM/2-FSK/2-PAM, β=0.5, η^*=1 bit/s/Hz

(b) 16-PPM/2-FSK/4-PAM, β=0.05, η^*=2 bit/s/Hz

Fig. 7. BER performance of different multi-dimensional modulations with optimal and sub-optimal receivers.

B. Trade off between computational complexity, spectral efficiency and error rate

Once identified the most suitable multi-dimensional modulation formats allowing the achievement of the considered target spectral efficiency, we pass now to investigate the performance of the proposed sub-optimal receivers. The results are still shown in terms of BER as a function of the SNR. Dealing with η^*=1 bit/s/Hz, Fig. 7(a) is related to 2-PPM/2-FSK/2-PAM with β=0.5, while Fig. 7(b) describes the performance of 16-PPM/2-FSK/4-PAM with β=0.05, related to η^*=2 bit/s/Hz. We have chosen such two modulation formats since characterized by different values of L, N and M that can impact on the receiver performance. For what concerns 2-PPM/2-FSK/2-PAM, Fig. 7(a) shows that QOR and OR guarantee the same reliability level, with the performance of FBR and DR being very close as well. This is due to the fact that, since L, N and M are equal to the lowest order possible, that is 2, the number of transmittable symbols is the lowest possible as well, hence reliability performance are less sensitive to the detection mechanism type. Regarding 16-PPM/2-FSK/4-PAM, as depicted in Fig. 7(b), the sub-optimal receivers still provide performance close to the optimum one. In this case where η^*=2 bit/s/Hz, symbol detection results as more challenging than for the previously investigated schemes. Therefore, having similar performance between optimal and sub-optimal solutions allows the receiver selection to be potentially performed basing on the computational effort constraints.

Following the remarks presented in Section III about the receiver selection, by means of the

TABLE I

COMPUTATION COST FOR QOR AND FBR.

Modulation scheme	Subopt. receiver	SNR γ 3 dB	6 dB	9 dB	12 dB
2-PPM/2-FSK/2-PAM	QOR	1.15	1.15	1.15	1.16
$\beta = 0.5$	FBR	1.01	1.00	1.00	0.99
16-PPM/4-FSK/2-PAM	QOR	0.49	0.47	0.46	0.45
$\beta = 0.05$	FBR	0.37	0.34	0.33	0.33
16-PPM/2-FSK/4-PAM	QOR	0.70	0.69	0.67	0.65
$\beta = 0.05$	FBR	0.64	0.63	0.61	0.61

proposed scheme we have the capability to select the most appropriate scheme to guarantee the quality of service achievement based on the propagation conditions, while selecting the less expensive approach from a computational point of view. In this direction, in order to evaluate the computational effort required by the proposed sub-optimal receivers with respect to the optimum one, we introduce now the metric $\mathcal{C}_d = \mathcal{O}_d/\mathcal{O}_{\text{OR}}$, measuring the processing effort required by the d-th receiver type (d = QOR,DR,FBR), normalized to the optimum receiver computational cost.

As discussed in Sec. III-C, the computational cost related to DR is fixed since depending only on L, N, M. Hence, for 2-PPM/2-FSK/2-PAM, 16-PPM/4-FSK/2-PAM and 16-PPM/2-FSK/4-PAM we have that $\mathcal{C}_{\text{DR}}$=1, $\mathcal{C}_{\text{DR}}$=0.333 and $\mathcal{C}_{\text{DR}}$=0.611, respectively. This means that, when dealing with 2-PPM/2-FSK/2-PAM, the processing complexity required by the DR is essentially the same of the OR, while for the cases 16-PPM/4-FSK/2-PAM and 16-PPM/2-FSK/4-PAM the use of DR allows a significant computational effort saving of about 70% and 40% with respect to the OR, respectively. On the other hand, the performance of QOR and FBR depends on the SNR impacting on eq. (12) and eq. (17). In this regard, Table I reports the results related to the considered QOR and FBR, measured at different SNR levels, and considering 2-PPM/2-FSK/2-PAM, 16-PPM/4-FSK/2-PAM and 16-PPM/2-FSK/4-PAM resulted as the best performing schemes from the previous analysis. Interestingly, it can be noted that, when dealing with 2-PPM/2-FSK/2-PAM, the sub-optimal receivers seem to be more costly than the optimum one. Such result is explained by the fact that, since L=2, the filtering operations for PPM-FSK detection required by QOR and FBR are essentially the same as for the OR. In fact, for QOR we

have that L_θ can be 1 or 2, thus very close or equal to L, while in FBR the running of a single feedback iteration leads the computational cost to be essentially the same as in the optimum case. Moreover, both QOR and FBR consider the implementation of an energy detector as initial stage of processing, that is not present in the OR. So, this is the reason why $\mathcal{C}_{\text{QOR}}$ and $\mathcal{C}_{\text{FBR}}$ are greater or equal to 1. Moving to 16-PPM/4-FSK/2-PAM and 16-PPM/2-FSK/4-PAM where L is very large, the processing saving provided by QOR and FBR (despite the implementation of the PPM energy detector) becomes remarkable since, in general, in QOR L_θ may be much smaller than L and in FBR the feedback iterations may be few. Specifically, in 16-PPM/4-FSK/2-PAM the cost of QOR is less than half of that one referred to the OR, while the cost of DR is even lower, with processing saving being larger than 60%. In the case of 16-PPM/2-FSK/4-PAM, representing a higher performing modulation since providing a spectral efficiency equal to 2 bit/s/Hz, the computational effort requested by QOR and DR increases. However, more than 30% of processing is avoided with respect to the OR case, and this result is still significant. Furthermore, the computational cost characterizing QOR and FBR tends to lower as the SNR grows, even though such decrease is only slight. In this regard, both 16-PPM/4-FSK/2-PAM and 16-PPM/2-FSK/4-PAM consider a very small β, so it follows that the PPM energy detector returns L values that are comparable in amplitude since PPM is far from be orthogonal. Hence, the number of filtering operations for QOR and FBR may not be the minimum one. On the other hand, by enlarging β the PPM detection results more reliable. As a consequence, in QOR L_θ tends to 1 and in FBR the feedback becomes rarely necessary (thus leading to the performance of DR).

Till now, we have slightly discussed about the role of β, anyway it is important to deeply explain its impact. As previously outlined, the use of a high PPM order as for 16-PPM/4-FSK/2-PAM and 16-PPM/2-FSK/4-PAM is made possible thanks to the realization of a non-orthogonal signaling with $\beta << 1$, allowing the spectral efficiency reduction due to L to be mitigated. By referring to the considered schemes, we now show in Fig. 8 how the choice of β rules the trade off between BER and spectral efficiency. Results have been obtained at γ=2.5 dB and γ=8dB for 16-PPM/4-FSK/2-PAM and 16-PPM/2-FSK/4-PAM, respectively, which represent the SNR conditions where a BER equal to 10^{-3} is achieved (see Fig. 6). Specifically, each point in Fig. 8 is characterized by a unique x coordinate, related to BER, and a double y coordinate related to β and η. Here, β is the independent variable (that is reported on the y-axis instead of the x-axis as in conventional plotting), while BER and η are the dependent ones. In fact, according

to eq. (5), there is a direct relationship between the values reported in the left y-axis (β) and in the right one (η) of Fig. 8. Furthermore, β impacts also on the reliability of PPM detection and on BER, reported on the x axis. By referring to Fig. 8(a) describing the performance of

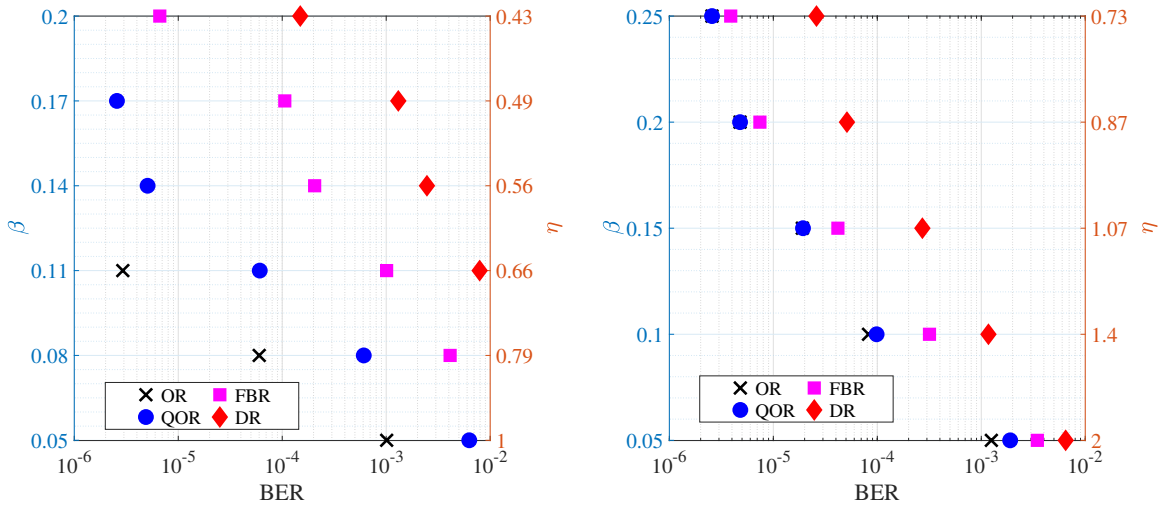

(a) 16-PPM/4-FSK/2-PAM (b) 16-PPM/2-FSK/4-PAM

Fig. 8. Performance trade off between BER and η^* as a function of β.

16-PPM/4-FSK/2-PAM providing η^*=1 bit/s/Hz, it is possible to appreciate that, for whatever detection mechanism employed at the receiver, BER lowers as β grows. When dealing with OR and QOR, the high reliability of the considered detection approaches allows the use of $\beta < 0.15$ to achieve a BER below 10^{-5}. On the other hand, for FBR and DR representing less complex solutions, a larger β would be required for performance improvement. Moving to the case 16-PPM/2-FSK/4-PAM providing η^*=2 bit/s/Hz, the performance of all the considered receivers follows essentially a similar behavior, with BER below 10^{-5} achievable only for $\beta > 0.2$. Of course, it can be verified from the right y-axis on Fig. 8 that the increase of β to improve the communication reliability is unavoidably paid in terms of spectral efficiency.

We recall that the main goal of our approach is to combine the robustness of PPM and FSK with the high spectral efficiency of PAM. By doing so, a more reliable communication can be achieved, without excessively sacrificing the data rate. This is what typically happens when coding is applied, with overhead being introduced to protect data from propagation errors, but by reducing rate. In this direction, we provide now a comparison with some multi-dimensional modulations and coded PAM schemes. Specifically, we considered BC with R=1/2 and R=1/3

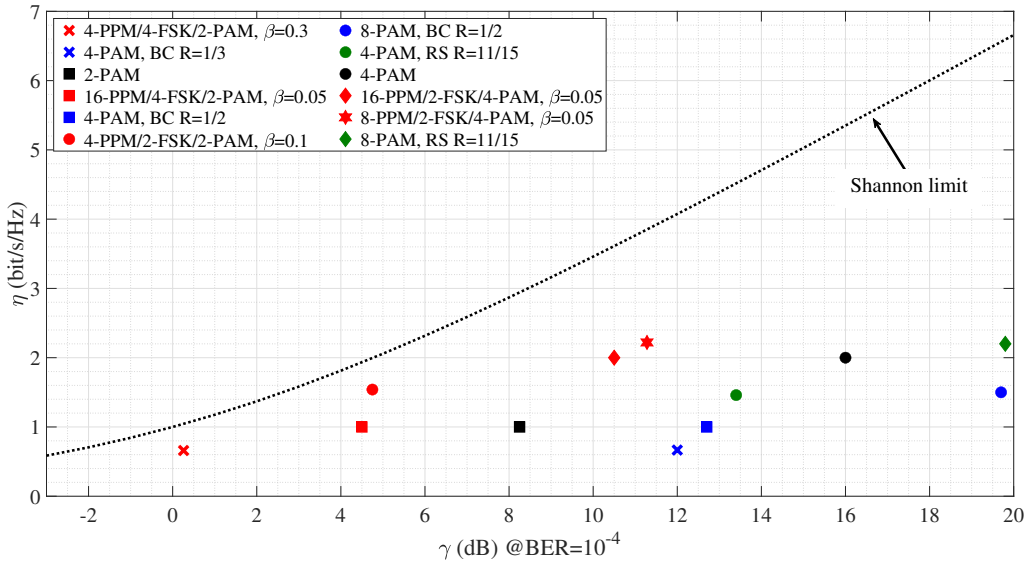

Fig. 9. Performance comparison between multi-dimensional schemes and coded modulations.

and Reed-Solomon (RS) coding with R=11/15, representing the most widespread techniques providing a good trade off between effectiveness and error protection complexity. Given the reference BER equal to 10^{-4}, we show in Fig. 9 a map where the points with coordinates (γ,η) describe the performance of the schemes under investigation. In Fig. 9, the multi-dimensional modulations are highlighted in red, pure PAM schemes in black, PAM with BC in blue and PAM with RS coding in green. Different modulation orders referred to the same scheme are instead differentiated with markers. For multi-dimensional modulations, we considered the performance achieved with the OR. Furthermore, Fig. 9 reports also the Shannon limit curve (note that the curve has not the typical logarithmic behavior as the SNR x-axis is on the logarithmic scale), so that it is possible to infer how close the modulations performance are with respect to the maximum achievable. Overall, it can be seen how the proposed multi-dimensional modulations outperform the other coded and uncoded PAM solutions. In fact, among same colored markers, those ones referring to multi-dimensional schemes are closer to the Shannon limit (see the squared red marker representing 16-PPM/4-FSK/2-PAM, the red circled marker describing 4-PPM/2-FSK/2-PAM and the red star-shaped marker related to 8-PPM/2-FSK/4-PAM). This means that, for a given pair of target BER and spectral efficiency to be provided, multi-dimensional modulations result as better performing in terms of SNR.

Finally, it is worth noting that the results shown in Fig. 9 allow multi-dimensional modulations and coding based solutions to be compared only from a communication point of view. Another fundamental benefit brought by multi-dimensional modulation concerns illumination, since the use of FSK signaling allows the average source output power to be constant, thus avoiding problem of dimming and flickering. On the other hand, when using PAM, with or without coding, despite the emitted symbols can be assumed as equiprobable, it is not possible to achieve lighting control, that may represent a severe limitation in indoor VLC scenarios where illumination and connectivity services must be simultaneously provided. To sum up the main results obtained in this section, we can highlight that multi-dimensional modulation scheme allows a dynamic and (computation)-cost efficient selection of the most suitable multi-dimensional scheme, with an eye on the power level of the light, to guarantee light levels homogeneity for users. This is a key point for deploying real-world VLC systems. In other words, with multi-dimensional modulation schemes, we aim to provide the most cost-effective solution by guaranteeing the quality of service imposed by the underlying applications. Another important consideration is regarding the energy efficiency, since as we can observe in Fig. 9, multi-dimensional modulations allow to achieve the same BER with a reduced SNR with respect to other coded and uncoded schemes, or otherwise said, at the same SNR level it is possible to reduce the BER, with an evident impact in terms of energy reduction. From this we can infer that the proposed modulation scheme allows to achieve higher energy efficiency.

C. Experimental validation

In order to validate the feasibility of the proposed multi-dimensional modulation, we performed several experiments by realizing an ad hoc test-bed based on Software Defined paradigm (Fig. 10(a)). As described in the schematic diagram in Fig. 10(d), at transmit side the test signals have been generated through an Arduino 1 board, using a low level code in order to directly operate on the registers of the micro-controller and so avoiding unwanted latency which could prevent the correctness of the tests.

Data were transmitted by modulating the optical emission of a Kingbright 104500 10mm red LED array. Each light is controlled by a dedicated digital output of the board and the number of LED simultaneously turned on determines the output optical flux. This approach allows to easily implement the PAM modulation, avoiding non linearities due to the current-optical flux characteristic of the LED. Since each LED is characterized by a limited output power, the

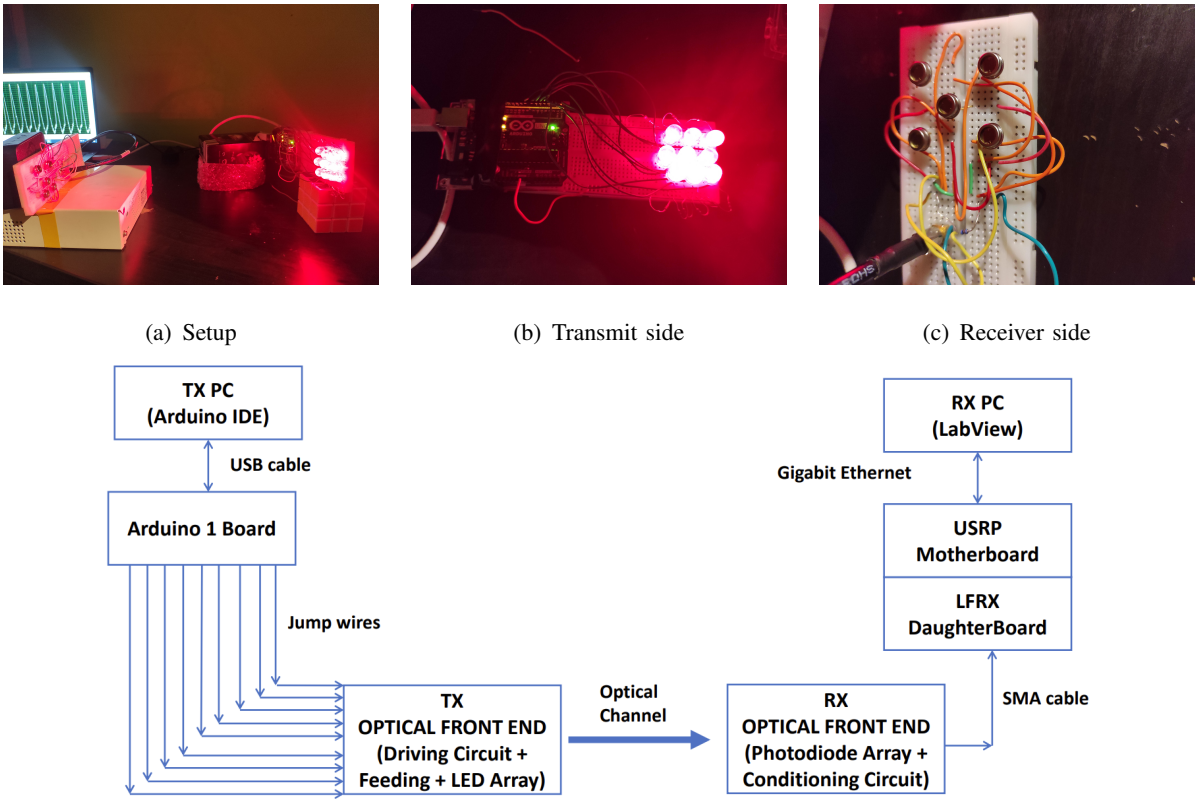

(a) Setup (b) Transmit side (c) Receiver side

(d) Schematic diagram

Fig. 10. Experimental setup description.

array configuration is also necessary to increase signal dynamics, achieve larger communication distances and maintain the proper average illumination level. In the experimental validation, we used 9 LEDs (Fig. 10(b)) in order to properly perform the PAM levels emission and generate the bias light level. At the receiver, the signal has been elaborated using a NI USRP 2920 and the commercial software LabView. In order to operate in base-band spectrum, a low frequency RX daughter-board, produced by Ettus, has been integrated between the optical receiver and the USRP motherboard. The optical receiver is composed of 5 CENTRONIC OSD15-5T PDs in order to realize a further gain and improve the quality of the received signal (Fig. 10(c)). All the PDs are arranged in parallel, acting as a unique current generator. Despite we actually realized a Multiple-Input Multiple-Output configuration, LEDs and PDs alignment has been accurately performed so as to let the system acting in Single-Input Single-Output mode. This is because using a single LED does not allow to generate reasonable power levels due to the LED characteristics (only 150mW power each). The received signal has not been amplified and

TABLE II

EXPERIMENTAL PARAMETERS

Receiver		Transmitter	
Photodiode Model	CENTRONIC OSD15-5T	LED Model	Kingbright RED 104500
Active Area	15 mm^2	Output Power	150 mW
Responsivity (620 nm)	0.4	Operative current	30 mA
Bandwidth	29.1 MHz	Light flux	1.4 lm
FOV	45°	FOV	80°
Rise time	12 ns	Forward current	30 mA

TABLE III

BER COMPARISON BETWEEN SIMULATION AND EXPERIMENT WITH OR AND QOR

Detection type	75 cm link (γ=13.9 dB)		175 cm link (γ=5.6 dB)	
	Sim.	Exp.	Sim.	Exp.
OR	$2 \cdot 10^{-7}$	$2.6 \cdot 10^{-7}$	$8.15 \cdot 10^{-3}$	$1.16 \cdot 10^{-2}$
QOR	$3.3 \cdot 10^{-7}$	$3.9 \cdot 10^{-7}$	$1.45 \cdot 10^{-2}$	$2.03 \cdot 10^{-2}$

no filtering operations have been performed. The transimpedance operation has been guaranteed just using a $1M\Omega$ resistor. Other information about the receiver and the transmitter are resumed in Table II. The experimental validation concerned 16-PPM/2-FSK/4-PAM with β=0.05, chosen since representing the most efficient scheme in terms of spectral efficiency and reliability among those ones previously investigated.

In detail, we evaluated the communication performance by transmitting a sequence of 10^8 symbols over two different link distances, that are 175 cm and 75 cm, where we measured a SNR equal to 5.6 dB and 13.9 dB, respectively. Regarding signal detection, we implemented the optimum receiver and the QOR, with this latter demonstrating to be the most effective sub-optimal detector. The results, expressed in terms of BER, are reported in Table III. For the two considered receivers and communication distances, we compared the BER values achieved with simulations and experiments. Specifically, it is possible to appreciate that test results only slightly

differ from those ones related to simulations. The really limited mismatch is due to the fact that the realized test-bed is not a pure single LED-single PD point-to-point link, so the propagation suffers from different angular emissions paths that are not accounted in the simulation model. However, it is possible to appreciate that at 75cm we achieve a BER of $3.3 \cdot 10^{-7}$ where the simulations report $2 \cdot 10^{-7}$. Obviously, at 175cm the BER is higher for both the cases (simulated and experiments) since the SNR is really low.

V. Conclusion

In this work we have proposed a novel joint modulation approach, based on different techniques, namely PAM, FSK and PPM. The main idea is to combine the different schemes in order to exploit their key features and limit the disadvantages of each modulation. The selection of the different schemes is based on the rationale that we can exploit in an effective way amplitude, frequency and time information. The combination of the different schemes is not trivial, and they have to be combined in order to keep a constant power level in a VLC system that is thought for illumination and communication simultaneously. In particular, we have proposed a framework that has been proven, both with a numerical evaluation and experimental results, to be effective and outperform block coding schemes. The proof of concept demonstrates the feasibility of the system, by the means of commercial components, such as LED and PDs, that do not require complex, ad-hoc hardware to integrate the framework. Performance results are very encouraging and prove not only the feasibility of such a kind of frameworks, but also the superiority in respect of block coding based approaches.

Acknowledgment

This publication has been based upon work from COST Action CA19111 NEWFOCUS, supported by COST (European Cooperation in Science and Technology).

References

[1] D. J. Langley, J. van Doorn, I. C. Ng, S. Stieglitz, A. Lazovik, and A. Boonstra, "The internet of everything: Smart things and their impact on business models," *Journal of Business Research*, vol. 122, pp. 853–863, 2021. [Online]. Available: https://www.sciencedirect.com/science/article/pii/S014829631930801X

[2] Z. Ghassemlooy, S. Arnon, M. Uysal, Z. Xu, and J. Cheng, "Emerging optical wireless communications-advances and challenges," *IEEE Journal on Selected Areas in Communications*, vol. 33, no. 9, pp. 1738–1749, 2015.

[3] Y. Zhang, L. Wang, K. Wang, K. S. Wong, and K. Wu, "Recent advances in the hardware of visible light communication," *IEEE Access*, vol. 7, pp. 91 093–91 104, 2019.

[4] D. Karunatilaka, F. Zafar, V. Kalavally, and R. Parthiban, "LED based indoor visible light communications: State of the art," *IEEE Communications Surveys & Tutorials*, vol. 17, no. 3, pp. 1649–1678, 2015.

[5] S. Doğan Tusha, A. Tusha, E. Basar, and H. Arslan, "Multidimensional index modulation for 5G and beyond wireless networks," *Proceedings of the IEEE*, vol. 109, no. 2, pp. 170–199, 2021.

[6] H. A. Ngo, C. Xu, S. Sugiura, and L. Hanzo, "Space-time-frequency shift keying for dispersive channels," *IEEE Signal Processing Letters*, vol. 18, no. 3, pp. 177–180, 2011.

[7] G. M. Yamga, A. R. Ndjiongue, and K. Ouahada, "Low complexity clipped frequency shift keying (FSK) for visible light communications," in *2018 IEEE 7th International Conference on Adaptive Science Technology (ICAST)*, 2018, pp. 1–6.

[8] R. Lee, K. Yun, J.-H. Yoo, S.-Y. Jung, and J. K. Kwon, "Performance analysis of M-ary PPM in dimmable visible light communications," in *2013 Fifth International Conference on Ubiquitous and Future Networks (ICUFN)*, 2013, pp. 380–383.

[9] S. Arnon, "The effect of clock jitter in visible light communication applications," *J. Lightwave Technol.*, vol. 30, no. 21, pp. 3434–3439, Nov 2012. [Online]. Available: http://opg.optica.org/jlt/abstract.cfm?URI=jlt-30-21-3434

[10] H. G. Batshon and I. B. Djordjevic, "Beyond 240 gb/s per wavelength optical transmission using coded hybrid subcarrier/amplitude/phase/polarization modulation," *IEEE Photonics Technology Letters*, vol. 22, no. 5, pp. 299–301, 2010.

[11] X. Liu, S. Chandrasekhar, T. H. Wood, R. W. Tkach, P. J. Winzer, E. C. Burrows, and A. R. Chraplyvy, "M-ary pulse-position modulation and frequency-shift keying with additional polarization/phase modulation for high-sensitivity optical transmission," *Opt. Express*, vol. 19, no. 26, pp. B868–B881, Dec 2011. [Online]. Available: http://opg.optica.org/oe/abstract.cfm?URI=oe-19-26-B868

[12] A. W. Azim, Y. Le Guennec, and L. Ros, "Hybrid Frequency and Phase-Shift Keying Modulation for Energy Efficient Optical Wireless Systems," *IEEE Wireless Communications Letters*, pp. 1–4, Nov. 2019. [Online]. Available: https://hal.archives-ouvertes.fr/hal-02383633

[13] M. A. Atta and A. Bermak, "A 160 m visible light communication link using hybrid undersampled phase-frequency shift on-off keying and CMOS image sensor," *Opt. Express*, vol. 27, no. 3, pp. 2478–2487, Feb 2019. [Online]. Available: http://opg.optica.org/oe/abstract.cfm?URI=oe-27-3-2478

[14] H. S. Khallaf, H. M. H. Shalaby, J. M. Garrido-Balsells, and S. Sampei, "Performance analysis of a hybrid QAM-MPPM technique over turbulence-free and gamma-gamma free-space optical channels," *Journal of Optical Communications and Networking*, vol. 9, no. 2, pp. 161–171, 2017.

[15] Y. Xu, Z. Chen, Z. Gong, Z. Xia, T. Yuan, Z. Gu, W. Zhao, and J. Chen, "Hybrid modulation scheme for visible light communication using CMOS camera," *Optics Communications*, vol. 440, pp. 89–94, 2019. [Online]. Available: https://www.sciencedirect.com/science/article/pii/S0030401819300550

[16] Z. Hua, T. Lu, Y. Huang, J. Zhang, S. Dang, and W. Zhao, "Three-dimensional constellation modulated visible light communications with pixelated addressable micro-LED array," in *2019 IEEE 2nd International Conference on Electronics and Communication Engineering (ICECE)*, 2019, pp. 172–177.

[17] T.-C. Bui, R. Singh, T. O'Farrell, and M. Biagi, "Energy-constrained slot-amplitude modulation with dimming support," *IEEE Photonics Technology Letters*, vol. 30, no. 14, pp. 1301–1304, 2018.

[18] ——, "Optical energy-constrained slot-amplitude modulation for dimmable vlc: Suboptimal detection and performance evaluation," *IEEE Transactions on Wireless Communications*, vol. 20, no. 3, pp. 1582–1595, 2021.

[19] J. G. Proakis and M. Salehi, *Digital Communications*, 5th ed. McGraw-Hill, 2008.

[20] A. Petroni, G. Scarano, R. Cusani, and M. Biagi, "Modulation precoding for MISO visible light communications," *Journal of Lightwave Technology*, vol. 39, no. 17, pp. 5439–5448, 2021.

[21] J. Ma, J. He, J. Shi, J. He, Z. Zhou, and R. Deng, "Nonlinear compensation based on K-means clustering algorithm for nyquist PAM-4 VLC system," *IEEE Photonics Technology Letters*, vol. 31, no. 12, pp. 935–938, 2019.

[22] L. Wang, X. Wang, J. Kang, and C. P. Yue, "A 75-mb/s RGB PAM-4 visible light communication transceiver system with pre- and post-equalization," *Journal of Lightwave Technology*, vol. 39, no. 5, pp. 1381–1390, 2021.